Stability of a Temporally Evolving Natural Convection Boundary Layer

Junhao Ke[1]†, N. Williamson[1], S. W. Armfield[1], G. D. McBain[2] and S. E. Norris[3]

[1]School of Aerospace, Mechanical and Mechatronic Engineering, The University of Sydney, New South Wales, 2006, Australia

[2]Memjet North Ryde Pty Ltd, Macquarie Park, New South Wales, 2113, Australia

[3]Department of Mechanical Engineering, The University of Auckland, Auckland, 1010, New Zealand

(Received xx; revised xx; accepted xx)

The stability properties of a natural convection boundary layer (NCBL) adjacent to an isothermally heated vertical wall with Prandtl number 0.71 are numerically investigated in the configuration of a temporally evolving parallel flow. The instantaneous linear stability of the flow is first invesitgated by solving the eigenvalue problem with a 'frozen' base flow. The critical point is found to be $Gr_\delta = 454.2$ with the most unstable wavenumber of $k = 0.0544$, where Gr_δ is the Grashof number based on the velocity integral boundary layer thickness δ. Temporal responses of the discrete perturbation modes are numerically obtained by solving the two-dimensional linearised disturbance equations using a 'frozen' base flow as an initial-value problem at various Gr_δ. The resultant amplification rates of the discrete modes are compared with the quasi-steady eigenvalue analysis, and both two-dimensional and three dimensional full direct numerical simulations of the temporally evolving flow. The selective amplification that is commonly found in the spatially developing NCBL is also observed in the temporally evolving case. The amplification rate predicted by the linear theory compares well with the direct stability analysis from $Gr_\delta \sim 8500$ to a transition point of $Gr_\delta \sim 1.3\times10^4$, confirming the temporally evolving NCBL shares very similar instantaneous stability properties to the 'frozen' steady base flow in this range. The transition Grashof number also coincides with the sudden change in the base flow and the mean flow statistics. The direct simulations show the value of the transition Grashof number depends on the initial perturbation amplitude. After the transition point, the direct stability results diverge from the linear stability predictions as the non-linear mechanisms become important.

Key words:

1. Introduction

Thermally driven natural convection boundary layers (NCBL) commonly arise in natural and industrial flows. The stability of the NCBL is of interest as it addresses the initial stage of the infinitesimal disturbance development that later leads to the laminar–turbulent transition.

† Email address for correspondence: junhao.ke@sydney.edu.au

Eckert (1951) investigated the laminar spatially developing NCBL in air subjected to natural disturbances using an interferometer. That experimental work indicated the laminar boundary layer amplifies a band of frequencies before the flow undergoes transition. Similar behaviour, later termed selective amplification, was confirmed by several experimental investigations in steady, spatially developing NCBLs (Dring & Gebhart 1969; Knowles & Gebhart 1968; Mahajan & Gebhart 1979; Hieber & Gebhart 1971). Early theoretical studies were carried out by Plapp (1957) and Szewczyk (1962) with experimental support, followed by a numerical investigation by Kurtz & Crandall (1962) using a finite difference method.

The marginal stability curves to the spatially developing NCBL flow adjacent to an isothermal wall were obtained numerically by Nachtsheim (1963) for $Pr = 0.733$ and $Pr = 6.7$ with an iterative Newton–Raphson method. The resultant marginal stability results were in good agreement with the experimental results obtained by Szewczyk (1962), Eckert *et al.* (1955) and Kurtz (1961). Experimental work by Polymeropoulos & Gebhart (1967) and Knowles & Gebhart (1968) also demonstrated the validity of applying the parallel-flow linear stability theory to the NCBL flow along a vertical wall with constant heat flux. Knowles & Gebhart (1968) showed that the NCBL flow is more unstable to the two-dimensional disturbances than the three-dimensional disturbances using a similar method to that of Squire (1933). Dring & Gebhart (1968) extended this work by theoretically investigating further downstream locations away from the neutral curve. It was showed that the NCBL flow is sharply filtering for a narrow band of frequencies that amplify more strongly than the other frequencies. This frequency band, however, is much higher than the most unstable frequency at the critical point (i.e. the frequency that is amplified first). The results were confirmed by Dring & Gebhart (1969) in their experimental work. On the basis of the linear stability theory, Gill & Davey (1969) presented the linear stability results for a thermally stratified NCBL with Dirichlet boundary conditions. Their work was later extended by McBain *et al.* (2007) with Neumann boundary conditions, using both eigenvalue and direct stability analysis. It was found that the amplification of the infinitesimal disturbances are eventually limited by non-linear effects.

Little work has been dedicated to the stability of unsteady NCBLs. Joshi & Gebhart (1987) investigated the transient stability of a spatially developing (where the boundary layer thickness δ is growing in both time and space, in the presence of the leading edge effect) NCBL flow in water with constant heat flux using anemometer and thermocouple measurements. The experimental work demonstrated that at larger downstream distances the transient flow may become unstable and undergo laminar–turbulent transition in the purely conductive regime before the arrival of the leading edge signal. Krane & Gebhart (1993) further investigated the transient stability of such a one-dimensional flow ($Pr = 6.7$) by assuming a slowly varying base flow and employing a quasi-static formulation (initially proposed by Shen (1961)). The frequency which has the maximum amplification rate from their marginal stability results was found to be slightly lower than the observed frequency band in the experimental work by Joshi & Gebhart (1987). The inaccuracy of the quasi-steady flow formulation for impulsively started flows (Shen 1961) was suggested as the probable cause of this discrepancy. A similar numerical approach was adopted by Brooker *et al.* (2000), who investigated the transient stability properties of a NCBL at $Pr = 6.25$ and $Pr = 7$ in a square cavity both experimentally and numerically. The two-dimensional parabolic stability analysis showed that the temperature signal is amplified more strongly than the velocity signal in the cavity. Since the cavity is limited by the top and bottom walls, all the disturbances are quickly damped by the base flow near the presence of the top and bottom wall. Despite the quasi-static assumption in

the eigenvalue calculations, the numerical results are still in good agreement with their experimental measurements.

The present paper concerns the flow stability of a temporally developing NCBL adjacent to a vertical heated isothermal wall of infinite extent. Practically, such temporally developing flows are of crucial importance, in particular, to those start-up unsteady flows where the non-dimensional downstream distance $Ra_x = g\beta\theta x^3/\nu\kappa$ is very large and a parallel flow could exist for a significant amount of time before the arrival of the leading edge signal (Goldstein & Briggs 1964).

The paper is organized as follows: An overview and a mathematical description of the problem is given in §2. The instantaneous linear stability of the NCBL flow is examined as an eigenvalue problem in §3 and an initial-value problem in §4. The stability map is obtained via the eigenvalue calculations with the assumption of a steady base flow. Using the linearised disturbance equations, the initial-value problem is also solved by freezing the base flow. The resultant two-dimensional temporal responses of the artificial discrete modes demonstrate the selective amplification behaviour as in spatially developing flows.

The direct stability results are in good agreement with the eigenvalue analysis. Further direct stability analyses are carried out in §5 to incorporate the effects of the non-linearity and unsteadiness in the base flow. The resultant amplification rates are compared with the linear stability predictions. Section §6 briefly summarizes the findings in this paper.

2. Mathematical Description

2.1. *Problem Definition*

The problem under consideration is governed by the incompressible Navier–Stokes equations, together with the conservation of mass and energy. By employing the Boussinesq approximation, those equations, in dimensionless form, read:

$$\frac{\partial u_i}{\partial x_i} = 0, \tag{2.1a}$$

$$\frac{\partial u_i}{\partial t} + u_j \frac{\partial u_i}{\partial x_j} = -\frac{\partial p}{\partial x_i} + Pr \frac{\partial^2 u_i}{\partial x_j^2} + \theta\delta_{i1}, \tag{2.1b}$$

$$\frac{\partial \theta}{\partial t} + u_j \frac{\partial \theta}{\partial x_j} = \frac{\partial^2 \theta}{\partial x_j^2}, \tag{2.1c}$$

where the subscripts $i, j = 1, 2, 3$ represent the x, y, z axes, in which directions are stream-wise, wall-normal and span-wise respectively, δ_{i1} denotes the Kronecker delta, i.e. $\delta_{i1} = 1$ if $i = 1$ otherwise $\delta_{i1} = 0$. The gravitational vector g is in the negative x direction, as depicted in the schematic sketch in figure 1. The Prandtl number $Pr = \nu/\kappa = 0.71$ is given by the ratio of the viscosity ν to the thermal diffusivity κ. Temperature is made dimensionless with the temperature difference $\Delta T = T_w - T_\infty$, i.e. $\theta = (T - T_\infty)/\Delta T$. The problem under consideration has no natural length scale as the isothermal wall extends indefinitely in both stream-wise (x) and span-wise (z) directions. The intrinsic length scale $L_s = \kappa^{2/3}/(g\beta\Delta T)^{1/3}$, time scale $t_s = \kappa^{1/3}/(g\beta\Delta T)^{2/3}$ and velocity scale $U_s = (\kappa g\beta\Delta T)^{1/3}$ are therefore employed to non-dimensionalize the other terms in equation (2.1) accordingly.

2.2. *Linearised Disturbance Equations*

We initially examine the characteristics of the two-dimensional linearised system. Two-dimensional perturbations $(\tilde{u}, \tilde{v}, \tilde{p}, \tilde{\theta})$ are superimposed upon the flow system by

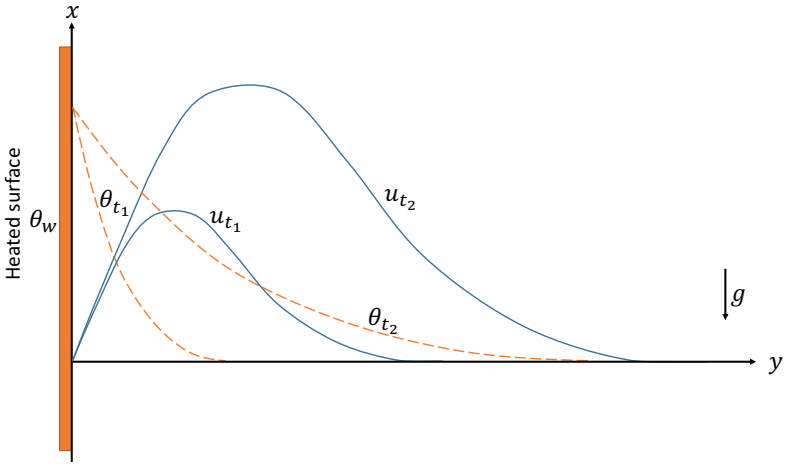

FIGURE 1. The development of the unsteady natural convection boundary layer profiles (non-dimensional stream-wise velocity u in solid lines and temperature θ in dashed lines) at two different time instants t_1 and t_2, with $t_2 > t_1$

substituting $u = U_b + \tilde{u}$, $v = \tilde{v}$, $p = p_b + \tilde{p}$, $\theta = \theta_b + \tilde{\theta}$ into the governing equation (2.1), where the subscript b denotes the instantaneous base flow profiles. After omitting the time variation in the base flow and higher-order non-linear terms, the dimensionless linearised disturbance equations (LDE) are obtained as:

$$\frac{\partial \tilde{u}}{\partial x} + \frac{\partial \tilde{v}}{\partial y} = 0, \tag{2.2a}$$

$$\frac{\partial \tilde{u}}{\partial t} + U_b \frac{\partial \tilde{u}}{\partial x} + \tilde{v} \frac{\partial U_b}{\partial y} = -\frac{\partial \tilde{p}}{\partial x} + Pr\left(\frac{\partial^2 \tilde{u}}{\partial x^2} + \frac{\partial^2 \tilde{u}}{\partial y^2}\right) + \tilde{\theta}, \tag{2.2b}$$

$$\frac{\partial \tilde{v}}{\partial t} + U_b \frac{\partial \tilde{v}}{\partial x} = -\frac{\partial \tilde{p}}{\partial y} + Pr\left(\frac{\partial^2 \tilde{v}}{\partial x^2} + \frac{\partial^2 \tilde{v}}{\partial y^2}\right), \tag{2.2c}$$

$$\frac{\partial \tilde{\theta}}{\partial t} + U_b \frac{\partial \tilde{\theta}}{\partial x} + \tilde{v} \frac{\partial \theta_b}{\partial y} = \frac{\partial^2 \tilde{\theta}}{\partial x^2} + \frac{\partial^2 \tilde{\theta}}{\partial y^2}. \tag{2.2d}$$

The validity of Squire's theorem was demonstrated by Knowles & Gebhart (1968) for the temporal stability analysis of a spatially developing NCBL flow, so the two-dimensional system (2.2) is expected to be most unstable to two-dimensional perturbations.

The base flow profiles U_b and θ_b are prescribed by the laminar analytical solution to the flow system (2.1), given by Illingworth (1950) and Schetz & Eichhorn (1962) at some desired t or Gr_δ. For $Pr \neq 1$, the analytical solution can be expressed in the dimensionless form:

$$\theta_b(\eta) = \mathrm{erfc}(\eta), \tag{2.3a}$$

$$U_b(\eta, t) = \frac{4t}{1 - Pr}\left[\mathrm{i}^2\mathrm{erfc}(\eta) - \mathrm{i}^2\mathrm{erfc}\left(\frac{\eta}{\sqrt{Pr}}\right)\right], \tag{2.3b}$$

where $\eta = y/2\sqrt{t}$ is a similarity parameter, $\mathrm{erf}(\eta)$ is the error function of η, $\mathrm{erfc}(\eta) = 1 - \mathrm{erf}(\eta)$ is the complementary error function and $\mathrm{i}^n\mathrm{erfc}(\eta)$ is the nth integral of the complementary error function: $\mathrm{ierfc}(\eta) = \exp(-\eta^2)/\sqrt{\pi} - \eta\mathrm{erfc}(\eta)$ and $\mathrm{i}^2\mathrm{erfc}(\eta) = \Big(\mathrm{erfc}(\eta) - 2\eta\mathrm{ierfc}(\eta)\Big)/4$. In the present study, the boundary layer thickness δ is defined

by the integral of the velocity profile over the maximum velocity U_m:

$$\delta = \int_0^\infty \frac{u}{U_m} \mathrm{d}y, \tag{2.4}$$

and $Gr_\delta = g\beta\Delta T\delta^3/\nu^2$ denotes the Grashof number based on the velocity integral boundary layer thickness δ.

3. Eigenvalue Results

3.1. *Quasi-Steady Approximation*

Eigenvalue analysis is commonly used to analyse the linear stability of steady base flows. To obtain an exponential disturbance growth, a steady base flow profile (constant U_b and θ_b in the disturbance equations (2.2)) is required. In the present study, the base flow is 'frozen' at some arbitrary non-dimensional time t so that a steady base flow profile is obtained.

Since the base flow thermal boundary layer thickness has a length scale of $t^{1/2}$ depending on the non-dimensional time t (Patterson & Imberger 1980), the thermal boundary layer evolves with a time scale of

$$\left(\frac{1}{t^{1/2}}\frac{\partial t^{1/2}}{\partial t}\right)^{-1} = 2t, \tag{3.1}$$

and the perturbation quantities evolve with a time scale of

$$\left(\frac{1}{A_t}\frac{\partial A_t}{\partial t}\right)^{-1} = \frac{1}{\sigma_k}, \tag{3.2}$$

where A_t is the amplitude of the perturbation and σ_k denotes the amplification rate of wavenumber k. The quasi-steady approximation may be justified by the argument that the time scale of the evolution of the base flow and that of the perturbations are separated, i.e. the perturbations are independent of the timescale of the evolution of the base flow when the time scale ratio $2t\sigma_k$ is large so that the base flow can be treated as a quasi-steady state.

This quasi-steady approximation for the unsteady temporally developing parallel boundary layer is analogous to the quasi-parallel approximation in the Orr–Sommerfeld equations for the steady spatially developing boundary layers (Gebhart & Mahajan 1982) and has been applied to the linear stability analyses for a temporally evolving Rayleigh layer problem (Otto 1993), an unsteady Stokes layer problem (Wu & Cowley 1995) and a time-dependent natural convection in a cavity (Brooker *et al.* 2000) with good accuracy.

3.2. *Freezing the Base Flow*

For the problem considered here, it is convenient to introduce a similarity coordinate in order to freeze the base flow:

$$\xi = \frac{x}{2\sqrt{t}}, \tag{3.3a}$$

$$\eta = \frac{y}{2\sqrt{t}}, \tag{3.3b}$$

$$\tau = {\tau_0}^{1/3} t, \tag{3.3c}$$

where τ_0 is an arbitrarily chosen constant at which time instant the base flow is 'frozen'.

Under these coordinates, the analytical laminar solutions (2.3) read:

$$\theta_b(\eta) = \mathrm{erfc}(\eta), \tag{3.4a}$$

$$U_b(\eta,\tau) \equiv V_b(\eta)\frac{\tau}{{\tau_0}^{1/3}} = \frac{4\tau}{(1-Pr){\tau_0}^{1/3}}\left[\mathrm{i}^2\mathrm{erfc}(\eta) - \mathrm{i}^2\mathrm{erfc}(\frac{\eta}{\sqrt{Pr}})\right], \tag{3.4b}$$

where V_b is a shape function of the velocity profile. From equation (3.4), the two-dimensional solution is dependent on time t (or $\tau/{\tau_0}^{1/3}$ equivalently) and is independent of stream-wise coordinate ξ. Since the unsteady temporally developing flow is parallel to the heated surface, the velocity integral boundary layer thickness δ as well as the Grashof number Gr_δ vary with the non-dimensional time t (or τ) only.

The velocity perturbations in equation (2.2) can be described by a perturbation stream function Ψ to ensure continuity, from which

$$\tilde{u} \equiv \frac{\partial\Psi}{\partial y} = \frac{\partial\Psi}{\partial\eta}\frac{\partial\eta}{\partial y}, \tag{3.5a}$$

$$\tilde{v} \equiv -\frac{\partial\Psi}{\partial x} = -\frac{\partial\Psi}{\partial\xi}\frac{\partial\xi}{\partial x}. \tag{3.5b}$$

The linear stability equations for the natural convection boundary layer are obtained after taking the out-of-plane component of the curl of the momentum equations (2.2b) and (2.2c).

$$\Big(\frac{\partial}{\partial\tau} - \frac{\xi}{2\tau}\frac{\partial}{\partial\xi} - \frac{\eta}{2\tau}\frac{\partial}{\partial\eta}\Big)\Delta\Psi + \frac{\tau^{1/2}}{2{\tau_0}^{1/2}}\Big(V_b\frac{\partial\Delta\Psi}{\partial\xi} - V_b''\frac{\partial\Psi}{\partial\xi}\Big) = \frac{Pr}{4\tau}\Delta^2\Psi + \frac{2\tau^{1/2}}{{\tau_0}^{1/2}}\frac{\partial\tilde{\theta}}{\partial\eta}, \tag{3.6a}$$

$$\Big(\frac{\partial}{\partial\tau} - \frac{\xi}{2\tau}\frac{\partial}{\partial\xi} - \frac{\eta}{2\tau}\frac{\partial}{\partial\eta}\Big)\tilde{\theta} + \frac{\tau^{1/2}}{2{\tau_0}^{1/2}}V_b\frac{\partial\tilde{\theta}}{\partial\xi} - \frac{{\theta_b}'}{4\tau}\frac{\partial\Psi}{\partial\xi} = \frac{1}{4\tau}\Delta\tilde{\theta}, \tag{3.6b}$$

where the prime $'$ denotes the differentiation with respect to η, and

$$\Delta = \frac{\partial^2}{\partial\xi^2} + \frac{\partial^2}{\partial\eta^2}, \tag{3.7}$$

For large enough τ, the first terms in equations (3.6) can be simplified as:

$$\frac{\partial}{\partial\tau} - \frac{\xi}{2\tau}\frac{\partial}{\partial\xi} - \frac{\eta}{2\tau}\frac{\partial}{\partial\eta} \sim \frac{\partial}{\partial\tau}. \tag{3.8}$$

It is noted that the conduction and viscous terms are retained even though they have the same asymptotic behaviour. Nevertheless, consider the perturbation normal modes given in equation (3.9):

$$\Psi = \psi(\eta)e^{\mathrm{i}\alpha(\xi-c\tau)}, \tag{3.9}$$

where $\mathrm{i} = \sqrt{-1}$ is the imaginary unit, $\alpha = 2\sqrt{t}k$ denotes the normalized wavenumber and ψ is the amplitude of the stream function. The imaginary part c_i of the complex number $c = c_\mathrm{r} + \mathrm{i}c_\mathrm{i}$ determines whether the perturbation wave α will be amplified ($c_\mathrm{i} > 0$) or damped ($c_\mathrm{i} < 0$) in time by the base flow, while the real part c_r indicates phase speed of the wave α.

The temperature perturbation can also be described in a similar form using the amplitude function of the temperature perturbation s:

$$\tilde{\theta} = s(\eta)e^{\mathrm{i}\alpha(\xi-c\tau)}. \tag{3.10}$$

The flow is then frozen at $\tau = \tau_0$ (so that $t_0 = {\tau_0}^{2/3}$, where t_0 is the non-dimensional

time instant in the intrinsic scale) after the substitution of equations (3.9) and (3.10) into (3.6). The stability equations are obtained as

$$i\alpha\Big[\big(\frac{V_b}{2}-c\big)(\psi''-\alpha^2\psi)-\frac{V_b''}{2}\psi\Big]=\frac{Pr}{4\tau_0}\big(\psi''''-2\alpha^2\psi''+\alpha^4\psi\big)+2s', \tag{3.11a}$$

$$i\alpha\Big[\big(\frac{V_b}{2}-c\big)s-\frac{1}{4\tau_0}\theta_b'\psi\Big]=\frac{1}{4\tau_0}(s''-\alpha^2 s). \tag{3.11b}$$

The resulting equations (3.11) are solved for the complex number c, which permits non-zero solutions for s and ψ at given positive α and τ_0 (equivalently, Gr_δ), as an eigenvalue problem. The amplification rate in the intrinsic scale is therefore

$$\sigma_k={\tau_0}^{1/3}\alpha c_{\rm i}={t_0}^{1/2}\alpha c_{\rm i}. \tag{3.12}$$

For the isothermal vertical plate, the boundary conditions are defined for the perturbations:

$$\psi(0)=\psi'(0)=s(0)=0, \tag{3.13a}$$

$$\psi(\infty)=\psi'(\infty)=s(\infty)=0. \tag{3.13b}$$

The velocity perturbations must vanish at the vertical wall (impermeability & non-slip conditions) and the temperature perturbation goes to zero at the isothermal wall. In the far field, both temperature and velocity perturbations should decay towards zero so that the perturbation is confined to the boundary layer.

3.3. *Eigenvalue Solutions*

Solutions to the linear stability equations (3.11) are obtained by solving the eigenvalue problem with varying τ_0 and α using the generalized Schur decomposition ('QZ') algorithm. The second-order finite difference method is used to numerically discretize the equations. Implementing the boundary conditions given in (3.13), calculation is carried out in a domain size of $0<\eta<10$ with $N_y=1024$ uniformly distributed nodes. Domain and grid size dependency tests are carried out to ensure a reliable solution.

In order to compare with the direct simulation results, the τ_0-dependent eigenvalue solutions are also presented in terms of Gr_δ. Here, the boundary layer thickness is given by

$$\delta\equiv\int_0^\infty\frac{U_b}{U_m}{\rm d}y=\int_0^\infty\frac{U_b}{U_m}{\rm d}\eta\frac{\partial y}{\partial\eta}=2\mathcal{C}{\tau_0}^{1/3}, \tag{3.14}$$

where

$$\mathcal{C}=\frac{4\int_0^\infty\big[{\rm i}^2{\rm erfc}(\eta)-{\rm i}^2{\rm erfc}(\eta/\sqrt{Pr})\big]{\rm d}\eta}{{\rm erfc}(\eta_m)-{\rm erfc}(\eta_m/\sqrt{Pr})}\sim 0.855, \tag{3.15}$$

is a constant since the base flow velocity profile U_b and the maximum velocity U_m are both linearly proportional to time in the similarity coordinate, and η_m is the maximum velocity location that satisfies:

$$\sqrt{Pr}\,{\rm ierfc}(\eta_m)={\rm ierfc}(\frac{\eta_m}{\sqrt{Pr}}). \tag{3.16}$$

Hence, the Grashof number is given by:

$$Gr_\delta=\frac{8\mathcal{C}^3}{Pr^2}\tau_0. \tag{3.17}$$

The evolution of the base flow boundary layer is therefore slow when compared with the

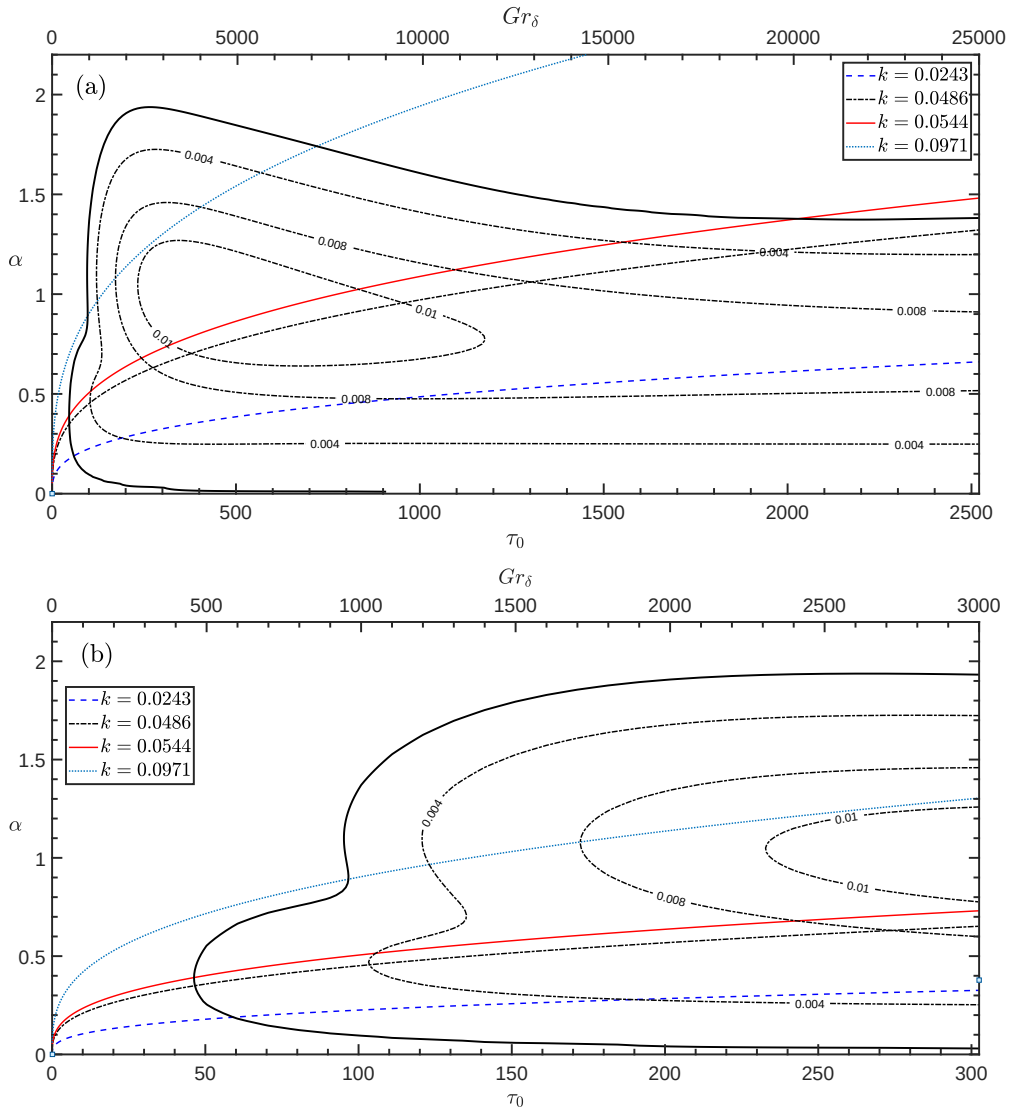

FIGURE 2. Linear stability margin of the temporally evolving NCBL for $Pr = 0.71$; (a): Marginal stability plane; (b): Enlarged near the critical point; black solid: Neutral curve, where $\alpha c_\mathrm{i} = 0$; dash-dotted contours: constant amplification rate $\alpha c_\mathrm{i} = 0.004$, $\alpha c_\mathrm{i} = 0.008$, and $\alpha c_\mathrm{i} = 0.01$; with constant wavenumber k trajectories in the marginal stability plane, blue dashed: $k = 0.0243$; black dash-dotted: $k = 0.0486$; red solid: $k = 0.0544$; turquoise dotted: $k = 0.0971$;

perturbation evolutions when the time scale ratio

$$2t\sigma_k = 2\alpha c_\mathrm{i}\tau_0 \sim O(Gr_\delta), \tag{3.18}$$

is large enough.

The resulting stability margin for $Pr = 0.71$ is shown in figure 2 with the trajectories of the constant wavenumber k. It shows that the base flow at given Gr_δ is unstable to a range of wavenumbers and selectively amplifies the perturbations, similarly to the spatially developing cases in Mahajan & Gebhart (1979) and Qureshi & Gebhart (1978). The maximum amplification rates ($\alpha c_\mathrm{i} \geqslant 0.01$) can be found in a core region between

$Gr_\delta \sim 2300$ and $Gr_\delta \sim 11700$ for a small band of frequencies from $k \sim 0.0337$ to $k \sim 0.0950$.

The critical point, that is the minimum τ_0 at which the base flow is linearly unstable, and the corresponding wavenumber and phase velocity are $\tau_0 = 45.7978$, $\alpha = 0.3894$ and $c = c_\mathrm{r} = 0.1193$ in the similarity coordinate, or more generally:

$$Gr_\delta = 454.2, \quad k = 0.0544, \quad U_p = 3.0551,$$

where $U_p = 2{\tau_0}^{2/3} c_\mathrm{r}$. On the other hand, in the spatially developing NCBL the critical point is found at a much higher Grashof number, i.e. $Gr_\delta = 642.9$ and $k = 0.0529$ (Nachtsheim 1963; Ostrach 1952). It is also interesting to find that at the critical point, the phase speed of the most unstable wavenumber U_p equals the maximum stream-wise velcoity U_m in the temporally evolving NCBL.

In figure 2 (a), the trajectory of the constant wavenumber at $k = 0.0971$ intersects the neutral curve at $Gr_\delta \sim 950$ and $Gr_\delta \sim 7000$. This suggests the discrete mode ($k = 0.0971$) follows a 'damped-amplified-damped' pathway, i.e. the disturbance wave first starts to be amplified at about $Gr_\delta \sim 950$, and is later damped from $Gr_\delta \sim 7000$. Similar behavior can be found for the most unstable wavenumber $k = 0.0544$ towards $Gr_\delta \sim 20000$. In contrast to the spatial cases (Dring & Gebhart 1968, 1969), the wavenumber which receives the maximum total amplification ς_{max} is not necessarily higher than the most unstable frequency at the critical point (in this case $k = 0.0544$), but is dependent on the pathway through the marginal stability map in figure 2. The total amplification is defined by equation (3.19):

$$\varsigma_k = \int_{Gr_{\delta_1}}^{Gr_{\delta_2}} \sigma_k(k, Gr_\delta) \mathrm{d}t. \tag{3.19}$$

Here, ς_k represents the total amplification of wavenumber k from Gr_{δ_1} to Gr_{δ_2}. Figure 3 depicts the total amplification of perturbation modes at $k = 0.0243$, $k = 0.0486$ and $k = 0.0971$ with a fixed starting point of $Gr_{\delta_1} = 250$. The discrete mode $k = 0.0486$ first becomes unstable to the base flow and receives the most amplification among the three modes up to $Gr_{\delta_2} \sim 2500$. After this range, the total amplification of the discrete mode $k = 0.0971$ outgrows that of $k = 0.0486$ for a short period. The most amplified frequency later switches back to $k = 0.0486$ since the instantaneous amplification rate of $k = 0.0971$ starts to drop at $Gr_{\delta_2} \sim 3500$, as indicated by figure 2. At about $Gr_{\delta_2} \sim 7000$, the total amplification of $k = 0.0971$ starts to decrease as the instantaneous amplification rate is negative (i.e. perturbation experiences damping).

4. Direct Solution to the LDE with 'Frozen' Base Flow

4.1. *Initial Value Problem on Two-Dimensional Frozen Base Flow*

The linear stability properties of the temporally evolving flow may also be obtained by a full solution of the perturbation equations. The linearised disturbance equations (2.2) are spatially discretized using the finite volume method. The non-linear advection terms are discretized by a fourth-order scheme, whilst all other spatial terms are second-order accurate. The second-order Adams–Bashforth method is adopted as the time stepping scheme with the Crank–Nicolson method used for the diffusive terms. The code has been extensively validated in a number of the natural convection problems (Williamson *et al.* 2012, 2016).

The stream-wise (x) boundaries are made periodic to eliminate the leading edge effect so that a temporally evolving flow is obtained. The velocity and the temperature perturbations are restricted by the non-slip and non-permeability boundary conditions

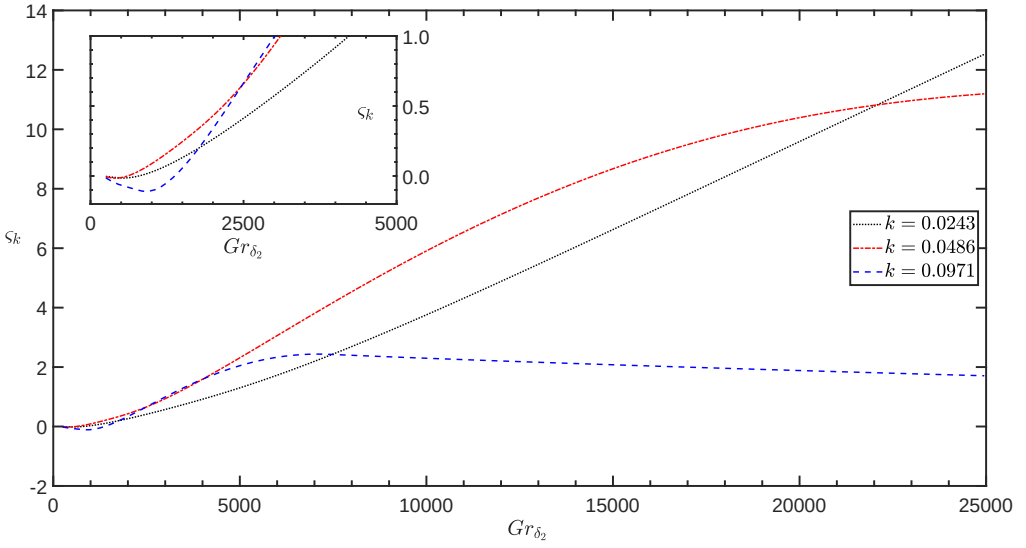

FIGURE 3. Total amplification of discrete modes of $k = 0.0243$ (black dotted), $k = 0.0486$ (red dash-dotted) and $k = 0.0971$ (blue dashed), with $Gr_{\delta_1} = 250$; Inset shows ς_k at small Gr_{δ_2}

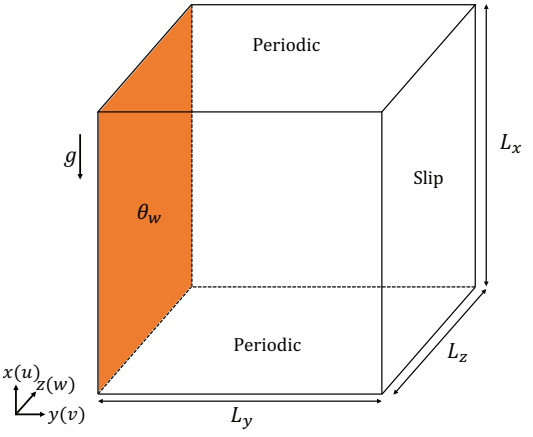

FIGURE 4. The computational domain and coordinates for the direct numerical simulations, the vertical isothermal wall is colored in orange

on the isothermal wall ($\tilde{u} = \tilde{v} = \tilde{\theta} = 0$ at $y = 0$). In the far field, both velocity and temperature perturbation decay, i.e. $\tilde{u} = \tilde{v} = \tilde{\theta} = 0$ at $y = L_y$. A schematic diagram of the simulation domain is shown in figure 4.

The base flow profiles U_b and θ_b are obtained as the laminar analytical solutions given by equation (2.3) at some desired base flow boundary layer Grashof number Gr_{δ_0}. To investigate the stability properties of the flow, the initialized base laminar boundary layer is augmented with a stream-wise temperature perturbation that decays in the wall-normal direction:

$$\tilde{\theta}_n = \theta_b(y) A_n \sin\left(2\pi n \frac{x}{L_x}\right), \tag{4.1}$$

where n is a real positive integer indicating the mode number (n/L_x) and the wavenumber ($k = 2\pi n/L_x$) of the sinusoidal perturbation. The amplitude of the temperature

perturbation A_n is selected so that the perturbation interacts with the base flow linearly, i.e. the amplification rate of the perturbation is independent of A_n. In the present study, it is chosen as $A_n = 10^{-3}$. It is noted that there is no velocity perturbation added to the flow as the velocity field is coupled to the temperature field and will respond directly to the temperature perturbation while remaining divergence free. The instantaneous linear stability of the unsteady flow is examined by integrating the linearised disturbance equations (2.2) for choices of perturbation wavenumber k in time for a 'frozen' (steady) base flow at time t (which is equivalent to the Grashof number based on the base flow boundary layer thickness Gr_δ) as an initial-value problem.

4.2. *Solutions to the Linearised Disturbance Equations*

The two-dimensional solutions to the disturbance equations are numerically obtained in a domain of $L_x \times L_y = 1035 \times 1035$ with a $N_x \times N_y = 1024 \times 1024$ Cartesian grid. The grid is uniform in the stream-wise (x) direction, but is geometrically stretched with a maximum stretching rate of $\gamma = 1.24\%$ in the wall-normal (y) direction. Additional simulations varying the domain size and the grid size were undertaken to ensure the solution is not adversely affected by the numerical settings.

The initial value problem is investigated by monitoring the time traces of the perturbation quantities $\tilde{\theta}$ and $\tilde{u}$ at an arbitrary fixed point (x_p,y_p) within the boundary layer. Given the base flow profiles U_b and θ_b at some instantaneous base flow Gr_{δ_0}, the flow is unstable to the perturbation of wavenumber k if the amplitude of the perturbation grows with time. Here, the subscript 0 indicates the initialization quantities.

The time traces in figure 5 show that the velocity and temperature perturbations have a constant phase difference, and the envelopes of the perturbation signals of wavenumber k should follow the exponential growth $A_n e^{\sigma_k t}$ (or decay, depending on the sign of σ_k) in time. The amplification rate σ_k is defined by

$$\sigma_k \equiv \frac{1}{A_t}\frac{\partial A_t}{\partial t}, \tag{4.2}$$

where the instantaneous perturbation amplitudes A_t, at time t, of the solutions to the linearised disturbance equations (2.2) are obtained by taking the fast Fourier transform in the stream-wise (x) direction of the perturbation quantities $\tilde{\theta}$ and $\tilde{u}$ at $y = y_p$. The development of A_t is depicted at four instances in figure 6, showing the temporal responses of the normal modes at different Gr_{δ_0}.

From figure 6, it is clear that the velocity and temperature perturbations share the same exponential slope, such that

$$\sigma_{k,\tilde{u}} = \sigma_{k,\tilde{\theta}} = \sigma_k, \tag{4.3}$$

for all k cases in the linear stage of the steady base flow. The normal modes are damped at small Gr_{δ_0}, as shown in figure 5 (a) and figure 6 (a). The laminar base flow is then filtering for a specific marginally unstable wavenumber ($\sigma_k = -0.0001 \sim 0$, see $k = 0.0486$ in (c) where the envelope is almost horizontal) at critical Gr_δ. With increasing Gr_δ, the range of discrete modes that are unstable to the base flow are broadened until all modes shown are amplified ($\sigma_k > 0$) by the base flow at different rates at $Gr_{\delta_0} = 1992.1$.

It is worth noting that there is always a region where the amplitude of the perturbation does not follow the linear growth/decay immediately after the disturbance is introduced into the base flow. This process, also known as receptivity, tunes the artificial perturbation to an appropriate initial amplitude and phase condition as the boundary layer receives the external disturbance (Morkovin 1969; Reed *et al.* 1996; Saric *et al.* 2002). The details

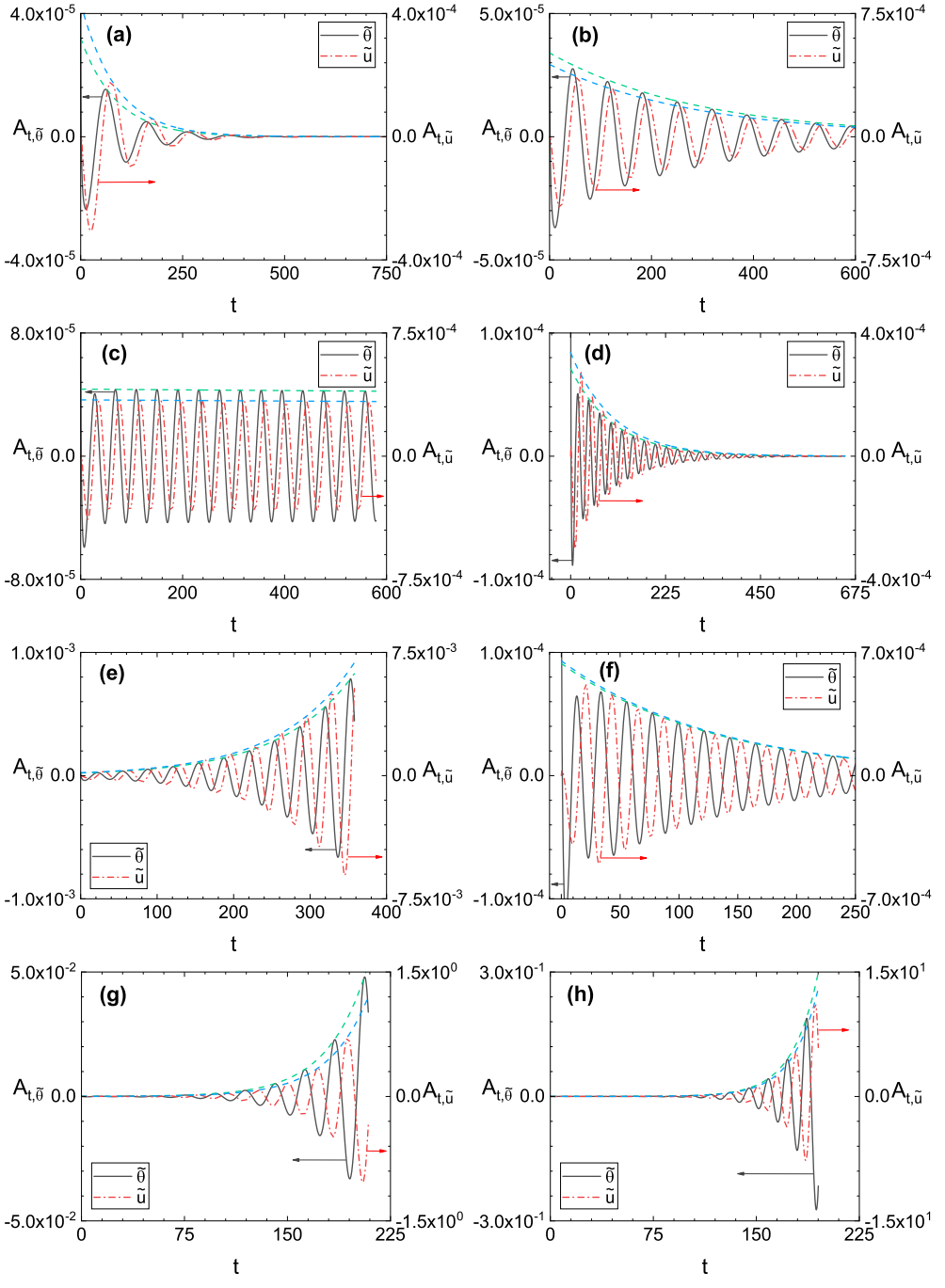

FIGURE 5. Time traces of the velocity and temperature perturbations $\tilde{\theta}$ (black solid), $\tilde{u}$ (red dash-dotted) at location (x_p, y_p)=(647.6, 0.2) for (a): Base flow at $Gr_{\delta_0} = 249.3$ and $k = 0.0243$ $(n = 4)$; (b): Base flow at $Gr_{\delta_0} = 454.3$ and $k = 0.0243$ $(n = 4)$; (c): Base flow at $Gr_{\delta_0} = 454.3$ and $k = 0.0486$ $(n = 8)$; (d): Base flow at $Gr_{\delta_0} = 454.3$ and $k = 0.0971$ $(n = 16)$; (e): Base flow at $Gr_{\delta_0} = 704.3$ and $k = 0.0486$ $(n = 8)$; (f): Base flow at $Gr_{\delta_0} = 704.3$ and $k = 0.0971$ $(n = 16)$; (g): Base flow at $Gr_{\delta_0} = 1992.1$ and $k = 0.0486$ $(n = 8)$; (h): Base flow at $Gr_{\delta_0} = 1992.1$ and $k = 0.0971$ $(n = 16)$; dashed lines: exponential envelopes of the signals

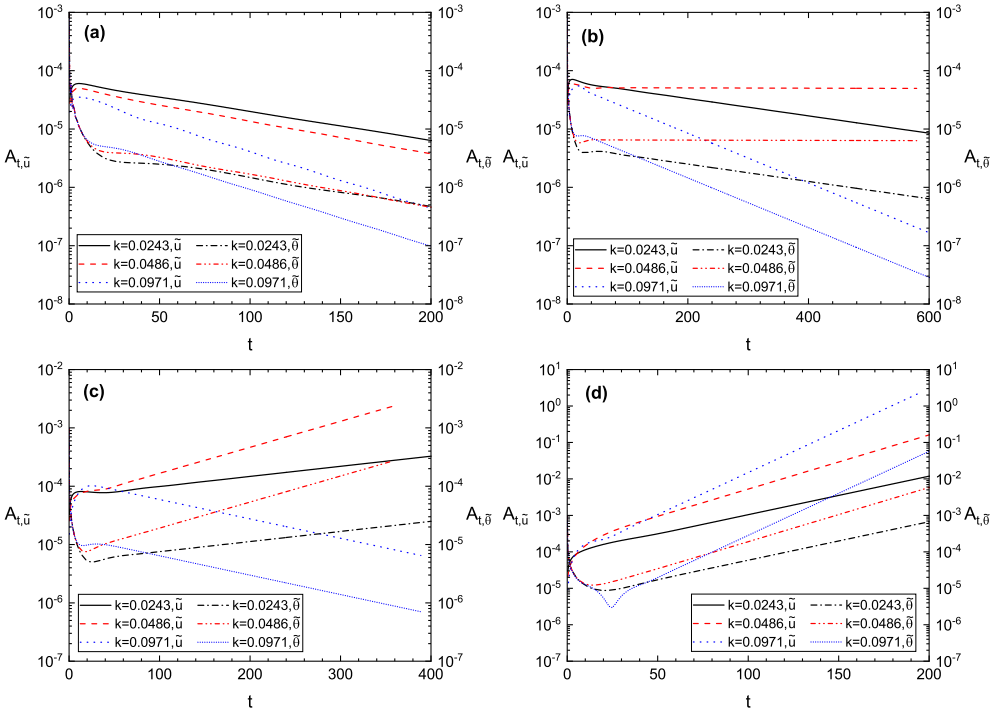

FIGURE 6. Time traces of the velocity and temperature perturbation amplitudes $A_{t,\tilde{u}}$ and $A_{t,\tilde{\theta}}$ at $y = y_p = 0.2$, 'frozen' base flow at (a): $Gr_{\delta_0} = 249.3$; (b): $Gr_{\delta_0} = 454.3$; (c): $Gr_{\delta_0} = 704.3$; (d): $Gr_{\delta_0} = 1992.1$;

Gr_{δ_0}	n	k	σ_k (LDE)	σ_k (ES)
454.3	4	0.0243	-0.0034	-0.0029
454.3	8	0.0486	-0.0001	-0.0002
454.3	16	0.0971	-0.0098	-0.0098
704.3	4	0.0243	0.0039	0.0034
704.3	8	0.0486	0.0103	0.0102
704.3	12	0.4454	0.0073	0.0073
704.3	16	0.0971	-0.0076	-0.0077
1992.1	4	0.0243	0.0243	0.0243
1992.1	8	0.0486	0.0343	0.0343
1992.1	12	0.4454	0.0494	0.0494
1992.1	16	0.0971	0.0532	0.0531

TABLE 1. Amplification rate σ_k for perturbation $\tilde{\theta}$ signals at given pairs of Gr_δ and k; LDE: Linearised disturbance equations; ES: Eigenvalue solutions

of the receptivity process, however, are beyond the scope of the present study. We shall only focus on the flow stability after the receptivity.

The detailed linear stability solutions to the 'frozen' base flows at given pairs of Gr_{δ_0} and k are tabulated in table 1. Both linearised disturbance solutions and eigenvalue calculations are in good agreement.

Case	Initial Condition	Perturbations	A_n	$N_x \times N_y(\times N_z)$	Δy_{min}	γ
DNS-A(2D)	$Gr_{\delta_0} = 249.3$	$k = 0.0243$	10^{-3}	1024×1024	2×10^{-4}	1.48%
DNS-B*(2D)	$Gr_{\delta_0} = 249.3$	$k = 0.0486$	10^{-3}	1024×1024	2×10^{-4}	1.48%
DNS-C(2D)	$Gr_{\delta_0} = 249.3$	$k = 0.0971$	10^{-3}	1024×1024	2×10^{-4}	1.48%
DNS-D(3D)	$Gr_{\delta_0} = 22.5$	$k = 0.0486$	10^{-3}	$1024 \times 512 \times 1024$	4.5×10^{-4}	3.56%
DNS-E(3D)	$Gr_{\delta_0} = 3000$	$k = 0.0486$	10^{-2}	$1024 \times 512 \times 1024$	4.5×10^{-4}	3.56%
DNS-F(3D)	$Gr_{\delta_0} = 3000$	Multi-modal	10^{-3}	$1024 \times 512 \times 1024$	4.5×10^{-4}	3.56%

TABLE 2. Simulation settings of the direct stability analyses; *: Both velocity and temperature fields are perturbed by pre-tuned perturbations from the linearised disturbance equations

5. Direct Numerical Simulation

5.1. *Direct Stability Analysis using Full Navier–Stokes Equation*

Using the same numerical techniques in §4, the full Navier–Stokes equations (2.1) are numerically solved in both two-dimensional and three-dimensional forms to incorporate the effects of the temporally evolving base flow and of nonlinearity on flow stability.

The boundary conditions for the velocity and temperature fields are the non-slip & isothermal non-permeable wall, i.e. $u = v = w = 0$ and $\theta_w = 1$ at $y = 0$ and the slip wall condition in the far field, i.e. $\frac{\partial u}{\partial y} = \frac{\partial \theta}{\partial y} = 0$ at $y = L_y$. Periodic boundaries are imposed in stream-wise and span-wise directions to allow a temporally evolving flow. Temporal responses of the perturbation waves are monitored and compared with the instantaneous linear stability solutions to address the unsteady effect of the base flow.

5.2. *Direct Numerical Simulation Results*

The direct numerical calculations are carried out in a domain of $L_x \times L_y(\times L_z) = 1035 \times 1035(\times 1035)$ with a non-staggered Cartesian grid. The grid is uniform in the stream-wise (x) and span-wise (z) directions, but is geometrically stretched with a maximum stretching rate of γ in the wall-normal (y) direction. Simulation settings are listed in table 2. To minimize the extent of the receptivity process, in case DNS-B both the temperature and velocity fields are perturbed with 'pre-tuned' perturbations from the linearised 'frozen base flow' simulation. For the two-dimensional simulation, temperature perturbations in the form of equation (4.1) are examined individually by looking at the temporal responses after feeding the discrete modes (initial perturbations) into the prescribed laminar base flow. In the present study, the two-dimensional simulations are initialized at $Gr_{\delta_0} = 249.3$ with discrete perturbation modes of $k = 0.0243$, $k = 0.0486$, and $k = 0.0971$. As the base flow profiles θ_b and U_b follow the laminar analytical solution (2.3), the perturbation quantities are sought to be $\tilde{\theta} = \theta - \theta_b$ and $\tilde{u} = u - U_b$. The resultant time traces show that the discrete modes $k = 0.0243$ and $k = 0.0486$, figures 7 (a-c), are amplified with time by the evolving base flow, whereas the perturbation at $k = 0.0971$, figure 7 (d), is damped out at about $Gr_\delta \sim 7000$ after a short period of amplification. Such behaviour confirms the discrete mode $k = 0.0971$ following the 'damped-amplified-damped' pathway as predicted by the 'quasi-steady' eigenvalue analysis results shown in figure 2.

At some large Gr_δ the unstable temporal signals (cases DNS-A and DNS-B) no longer follow the exponential growth of the sinusoidal signals, indicating non-linear behaviour as the boundary layer grows thicker. The development of the harmonics, which are usually generated by the non-linear interactions, are compared with that of the initial perturbations to investigate this non-linearity. As indicated by figure 8, the higher

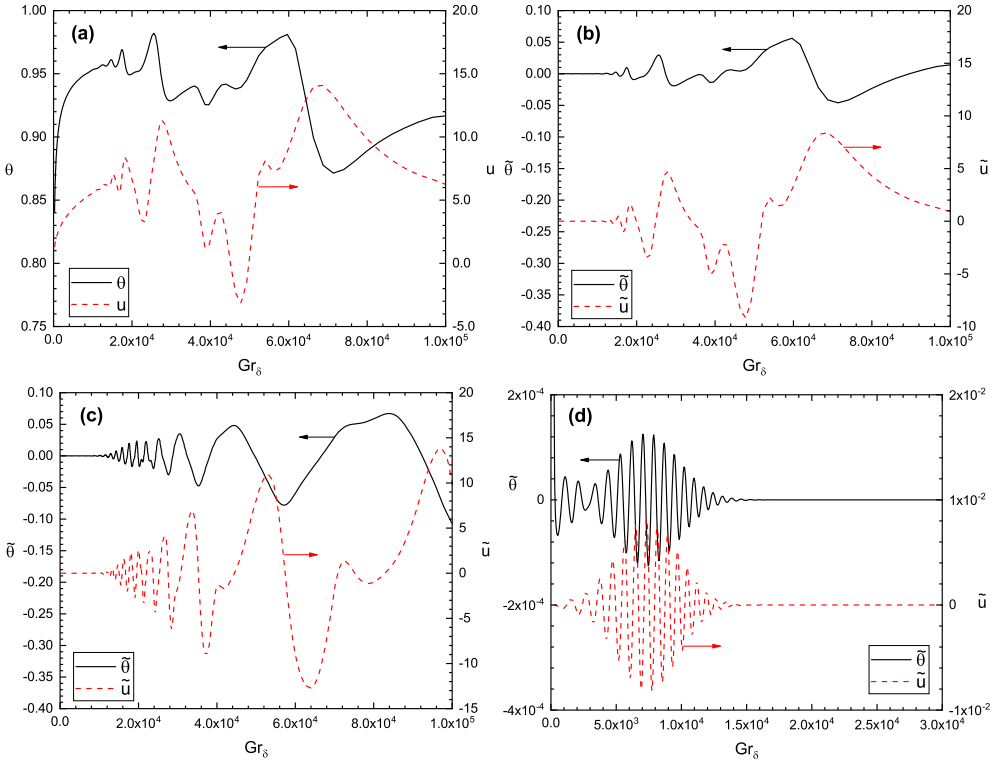

FIGURE 7. Time traces of the perturbation signals at point $(x_p,\ y_p)$=(647.6, 0.2) for (a): case DNS-A, raw signal (with base flow); (b): case DNS-A, perturbation signal (analytical base flow subtracted); (c): case DNS-B, perturbation signal (analytical base flow subtracted); (d): case DNS-C, perturbation signal (analytical base flow subtracted); black solid: Temperature signals; red dashed: velocity signals

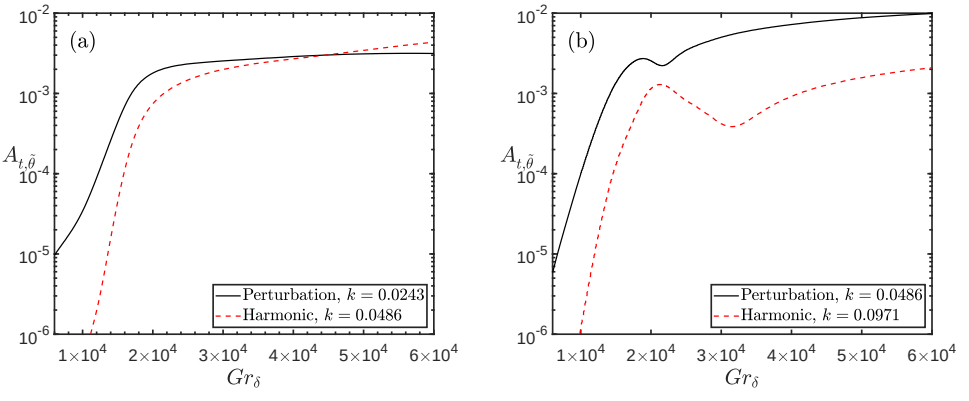

FIGURE 8. Development of the harmonics; (a): case DNS-A, initial perturbation $k = 0.0243$; (b): case DNS-B, initial perturbation $k = 0.0486$; black solid: perturbations; red dashed: harmonic waves

harmonics of the perturbation waves are both increasing their strength as the base flow continues to evolve. In figure 8 (a), the harmonic mode ($k = 0.0486$) grows rapidly and later overwhelms the initial perturbation at large Gr_δ, as the harmonic mode at $k = 0.0486$ is less stable to the base flow than the initial perturbation ($k = 0.0243$)

according to the marginal stability plane (figure 2). The harmonic mode in this case not only receives energy from the initial perturbation but also gets amplified by the base flow. In figure 8 (b), since the discrete mode at $k = 0.0971$ experiences damping for $Gr_\delta > 7000$ in the linear regime, the development of the harmonic mode ($k = 0.0971$) depends solely on the non-linear mechanisms. Consequently, the resultant non-linearity in the case DNS-A appears more powerful than in the case DNS-B (see also figure 7) as the harmonic wave is amplified much more quickly than the initial perturbation.

The temporal response of discrete wavenumber $k = 0.0486$ is also examined using three-dimensional direct simulations. To investigate the effect of the initial conditions, the laminar flow is initialized at $Gr_{\delta_0} = 22.5$ for case DNS-D and at $Gr_{\delta_0} = 3000$ for case DNS-E and case DNS-F. The amplitude of the finite disturbance is chosen as $A_n = 10^{-3}$ for case DNS-D and case DNS-F and $A_n = 10^{-2}$ for case DNS-E. In case DNS-F, multiple temperature normal modes, in the form of equation (5.1), are added to the base flow solution to thermally perturb the boundary layer:

$$\tilde{\theta}_x = \theta_b(y) A_n \sum_{r=0}^{7} \sin\left(2^r \frac{2\pi x}{L_x}\right), \tag{5.1}$$

where r is an integer specifying the components of the sinusoidal perturbation. While the base flow lies in the laminar linear regime, each of the individual components are expected to interact linearly with the base flow.

A random background white noise, given in equation (5.2), is also superposed on the initial temperature field to trigger the three-dimensional laminar–turbulent transition for case DNS-F (Nakao *et al.* 2017).

$$\tilde{\theta}_0 = A_0[\mathrm{RAND}(0,1) - 0.5], \tag{5.2}$$

where $A_0 = 10^{-6}$ is the amplitude of the background white noise and $\mathrm{RAND}(0,1)$ denotes a random number generator which generates statistically uniformly distributed random numbers between 0 and 1.

In figure 9, the amplification rate σ_k of the perturbation mode $k = 0.0486$ is compared with the linear stability results. Due to the inevitable receptivity, the perturbation does not follow the prediction of the linear stability analysis instantly but is tuned by the base flow to a suitable magnitude for a short period after it is introduced into the flow. Such receptivity effects can also be observed in DNS-B in figure 9 (a) where both temperature and velocity fields are perturbed by the solutions to the linearised disturbance equations, indicating the magnitude and phase relation obtained from the 'frozen base flow' no longer holds for the unsteady base flow due to the additional terms in the unsteady Navier–Stokes equations. Consequently, we are not able to determine the minimum value of τ_0 or equivalently, Gr_δ for which the quasi-steady approximation is valid, i.e. to what extent can Gr_δ be deemed as 'large enough' so that the slowly varying base flow assumption holds. At large Gr_δ, as depicted by figure 9, the amplification rate predicted by the quasi-steady eigenvalue analysis shows reasonably good agreement with the direct stability analysis in the linear range.

The two-dimensional simulation (case DNS-B) shows similar development to the three-dimensional simulations (case DNS-D and DNS-F) up to the initial stage of the non-linear behaviour (before the amplification rate reaches its minimum at around $Gr_\delta \sim 2 \times 10^4$ for case DNS-D and DNS-F). The velocity amplification rate ($\sigma_{\tilde{u}}$) is found slightly larger than that of the temperature ($\sigma_{\tilde{\theta}}$) in the linear region as shown in figure 9 (b), so that equation (4.3) does not hold for the unsteady base flow.

In cases DNS-B, D and F, at about $Gr_\delta \sim 1.3 \times 10^4$ the amplification rate obtained by

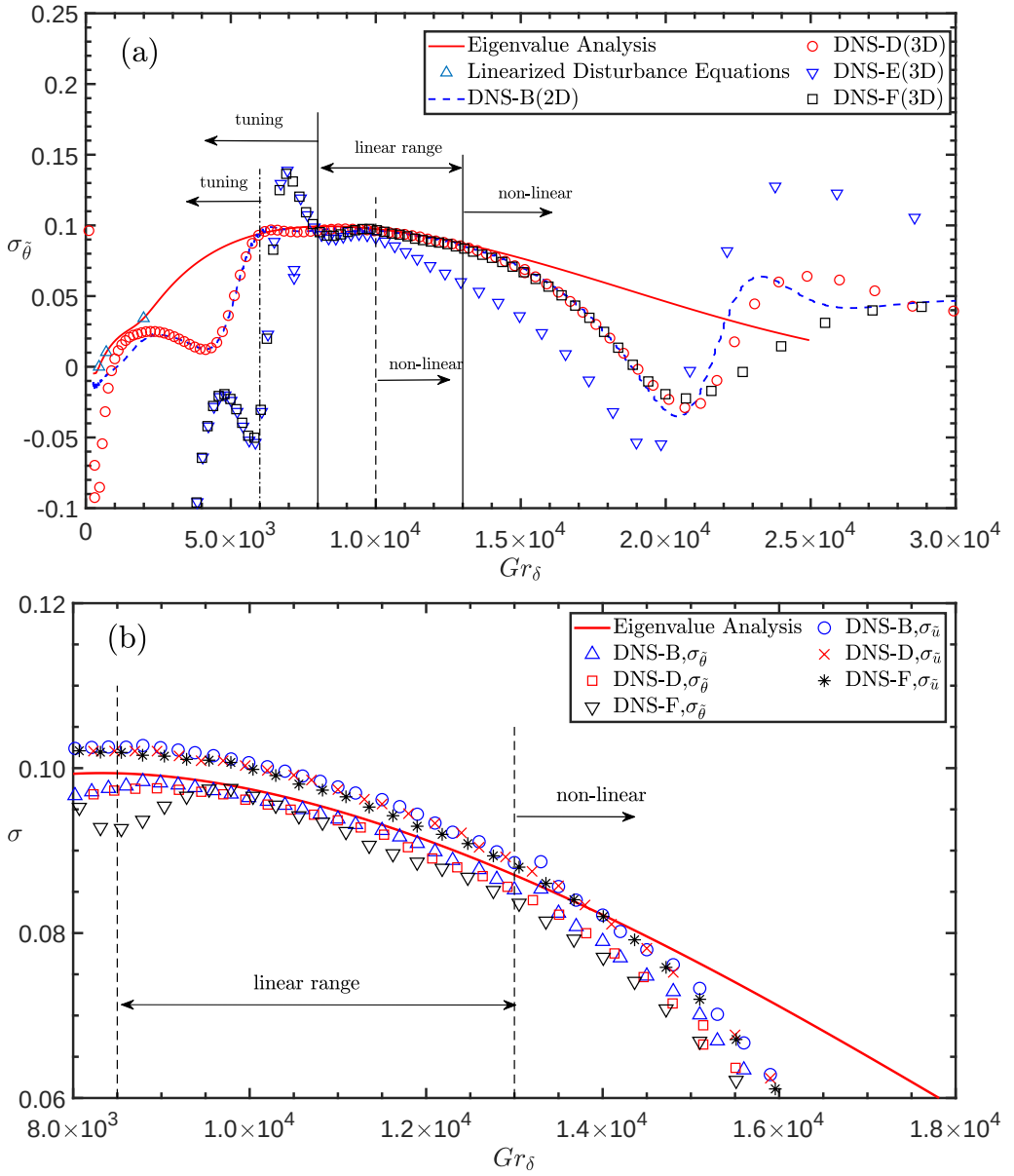

FIGURE 9. Amplification rate comparison for wavenumber $k = 0.0486$; (a): Temperature amplification rate; (b): Velocity and temperature amplification rate in the linear range of the unsteady flow (not all data are shown for clarity)

direct stability analysis differs from the eigenvalue solution, indicating the onset of the non-linearity. This Grashof number, on the other hand, coincides well with the sudden change in the mean flow statistics such as the wall shear stress and the Nusselt number, as shown in figure 10. Here, the wall shear stress $\tau_w = \nu \partial u/\partial y$ is normalized by

$$\tau_w{}^* = \tau_w/(\rho g \beta \theta_w \delta), \tag{5.3}$$

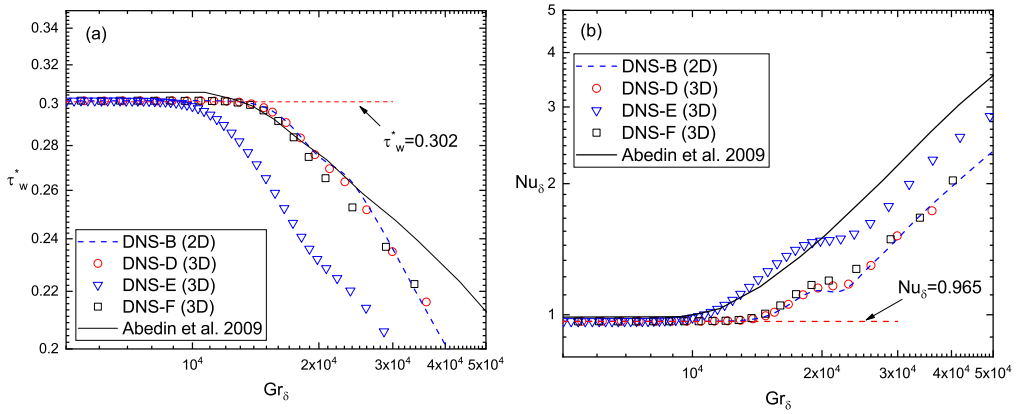

FIGURE 10. Mean flow statistics (not all data are shown for clarity), (a): normalized wall shear stress development; (b): the Nusselt number development;

and the Nusselt number is defined by

$$Nu_\delta = -\frac{\delta \frac{\partial \theta}{\partial y}|_{y=0}}{\theta_w}. \tag{5.4}$$

Since the mean flow velocity and temperature distribution follow the analytical solution (2.3), an analytical correlation of the normalized wall shear stress and the Nusselt number can be derived in equation (5.5)

$$Nu_\delta = \frac{\delta}{\sqrt{\pi t}} \sim 0.965, \tag{5.5a}$$

$$\tau^*_w = \frac{2\sqrt{Prt}}{\sqrt{\pi}\delta(\sqrt{Pr}+1)} \sim 0.302. \tag{5.5b}$$

A sudden drop of the wall shear stress from the analytical correlation can be found in figure 10 (a) whilst a sudden increase in the Nusselt number is observed in (b) at around the transition Grashof number. Similar behaviour is found in case DNS-E with a smaller Grashof number at around $Gr_\delta \sim 10^4$. Such sudden changes in the mean flow statistics were also observed in a DNS study for the temporally developing NCBL by Abedin *et al.* (2009) (also shown in figure 10) at around $Gr_\delta \sim 10^4$. This point is the critical Grashof number that indicates the onset of laminar–turbulent transition of the unsteady NCBL. From figure 9 and figure 10, it can be seen that the choice of the initialization of the laminar flow in terms of Gr_{δ_0} (at which time instant that the perturbations are fed into the laminar base flow) has minimal effect on the transition Grashof number. Nevertheless, the initial amplitude of the infinitesimal perturbation plays an important role in determining this parameter. A ten-fold increase in the initial perturbation amplitude leads to an earlier transition without having much effect in the tuning and linear range. The discrepancy between Abedin *et al.* (2009) and the present study may due to the settings, such as the perturbation modes, amplitude, span-wise (background) perturbations.

6. Conclusion

In this paper, the stability properties of an unsteady, temporally evolving NCBL adjacent to an isothermally heated vertical wall are investigated. The laminar base flow

is shown to be initially filtering for a specific marginally unstable wavenumber, and broadening to a range of unstable wavenumbers with increasing Gr_δ. At high enough Gr_δ in the linear region, the initially unstable modes are damped. The critical Gr_δ at which a single mode first become unstable is found to be lower than the corresponding critical Gr_δ for a spatially developing NCBL (Nachtsheim 1963). At the critical $Gr_\delta = 454.2$, the phase velocity U_p of the most unstable wavenumber ($k = 0.0544$) is found to be the same as the maximum velocity U_m of the base flow, which was also observed by Armfield & Patterson (1992). In contrast to the observations in the spatially developing NCBL flows (Dring & Gebhart 1968, 1969), the most amplified frequency is not necessarily higher than the initially unstable wavenumber ($k = 0.0544$), but strongly depends on the pathway through the marginal stability map. The amplification rate predicted by the eigenvalue analysis and direct numerical simulations is similar in the linear range (see figure 9), showing that the instantaneous stability properties of an unsteady, temporally evolving NCBL are very similar to those of a steady NCBL at the same local Gr_δ. However, the perturbation taken from the linearised 'frozen' base flow still undergoes the receptivity process (see case DNS-B), indicating the magnitude and phase relation of the perturbation obtained in the steady, linearised NCBL does not hold in the unsteady NCBL. By comparing the amplification rates, it is found that the amplification rate calculated from the direct stability analysis diverges from the linear stability predictions after a transition point. In contrast to the parabolic stability analysis for the two-dimensional square cavity case (Brooker *et al.* 2000), we found that the velocity signals are amplified at a slightly higher rate than the temperature signals in the linear region. The Grashof number at transition is found to be independent of the time that the perturbations are applied (in terms of Gr_δ), but is related to the initial amplitude of the perturbation. From the present study, the transition value is $Gr_\delta \sim 1 \times 10^4$ for $A_n = 10^{-2}$ and $Gr_\delta \sim 1.3 \times 10^4$ for $A_n = 10^{-3}$. The transition value also coincides with the sudden change in mean flow statistics that indicates laminar–turbulent transition, such as the wall shear stress and the Nusselt number.

REFERENCES

Abedin, M. Z, Tsuji, T. & Hattori, Y. 2009 Direct numerical simulation for a time-developing natural-convection boundary layer along a vertical flat plate. *Int. J. Heat Mass Transf.* **52** (19-20), 4525–4534.

Armfield, S. W. & Patterson, J. C. 1992 Wave properties of natural-convection boundary layers. *J. Fluid Mech.* **239**, 195–211.

Brooker, A. M. H., Patterson, J. C., Graham, T. & Schöpf, W. 2000 Convective instability in a time-dependent buoyancy driven boundary layer. *Int. J. Heat Mass Transf.* **43** (2), 297–310.

Dring, R. P. & Gebhart, B. 1968 A theoretical investigation of disturbance amplification in external laminar natural convection. *J. Fluid Mech.* **34** (3), 551–564.

Dring, R. P & Gebhart, B. 1969 An experimental investigation of disturbance amplification in external laminar natural convection flow. *J. Fluid Mech.* **36** (3), 447–464.

Eckert, E. R. G. 1951 Interferometric studies on the stability and transition to turbulence of a free convection boundary layer. *Proc. General Discussion on Heat Transfer* pp. 321–323.

Eckert, E. R. G., Soehngen, E. & Schneider, F. J. 1955 Studien zum umschlag laminar-turbulent der freien konvektions-stromung an einer senkrechten platte. *Anniversary volume Fiinfzig Jahre Grenzschichtforschung* pp. 407–418.

Gebhart, B. & Mahajan, R. L. 1982 Instability and transition in buoyancy-induced flows. In *Adv. Appl. Mech.*, , vol. 22, pp. 231–315. Elsevier.

Gill, A. E. & Davey, A. 1969 Instabilities of a buoyancy-driven system. *J. Fluid Mech.* **35** (4), 775–798.

Goldstein, R. J. & Briggs, D. G. 1964 Transient free convection about vertical plates and circular cylinders. *J. Heat Transfer* **86** (4), 490–500.

Hieber, C. A. & Gebhart, B. 1971 Stability of vertical natural convection boundary layers: some numerical solutions. *J. Fluid Mech.* **48** (4), 625–646.

Illingworth, C. R. 1950 Unsteady laminar flow of gas near an infinite flat plate. In *Math. Proc. Camb. Philos. Soc.*, , vol. 46, pp. 603–613. Cambridge University Press.

Joshi, Y. & Gebhart, B. 1987 Transition of transient vertical natural-convection flows in water. *J. Fluid Mech.* **179**, 407–438.

Knowles, C. P & Gebhart, B. 1968 The stability of the laminar natural convection boundary layer. *J. Fluid Mech.* **34** (4), 657–686.

Krane, M. J. M. & Gebhart, B. 1993 The hydrodynamic stability of a one-dimensional transient buoyancy-induced flow. *Int. J. Heat Mass Transf.* **36** (4), 977–988.

Kurtz, E. F. 1961 A study of the stability of laminar parallel flows. PhD thesis, Massachusetts Institute of Technology.

Kurtz, E. F. & Crandall, S. H. 1962 Computer-aided analysis of hydrodynamic stability. *J. Math. Phys.* **41** (1-4), 264–279.

Mahajan, R. L. & Gebhart, B. 1979 An experimental determination of transition limits in a vertical natural convection flow adjacent to a surface. *J. Fluid Mech.* **91** (1), 131–154.

McBain, G. D., Armfield, S. W. & Desrayaud, G. 2007 Instability of the buoyancy layer on an evenly heated vertical wall. *J. Fluid Mech.* **587**, 453–469.

Morkovin, M. V. 1969 On the many faces of transition. In *Viscous Drag Reduction*, pp. 1–31. Springer.

Nachtsheim, P. R. 1963 Stability of free-convection boundary-layer flows .

Nakao, K., Hattori, Y. & Suto, H. 2017 Numerical investigation of a spatially developing turbulent natural convection boundary layer along a vertical heated plate. *Int. J. Heat Fluid Flow* **63**, 128–138.

Ostrach, S. 1952 An analysis of laminar free-convection flow and heat transfer about a flat plate parallel to the direction of the generating body force. *Tech. Rep.*. National Aeronautics and Space Administration Cleveland Oh Lewis Research Center.

Otto, S. R. 1993 On the stability of a time dependent boundary layer .

Patterson, J. C. & Imberger, J. 1980 Unsteady natural convection in a rectangular cavity. *J. Fluid Mech.* **100** (1), 65–86.

Plapp, J. E. 1957 I. laminar boundary layer stability in free convection. PhD thesis, California Institute of Technology.

Polymeropoulos, C. E. & Gebhart, B. 1967 Incipient instability in free convection laminar boundary layers. *J. Fluid Mech.* **30** (2), 225–239.

Qureshi, Z. H. & Gebhart, B. 1978 Transition and transport in a buoyancy driven flow in water adjacent to a vertical uniform flux surface. *Int. J. Heat Mass Transf.* **21** (12), 1467–1479.

Reed, H. L., Saric, W. S. & Arnal, D. 1996 Linear stability theory applied to boundary layers. *Annu. Rev. Fluid Mech.* **28** (1), 389–428.

Saric, W. S., Reed, H. L. & Kerschen, E. J. 2002 Boundary-layer receptivity to freestream disturbances. *Annu. Rev. Fluid Mech.* **34** (1), 291–319.

Schetz, J. A. & Eichhorn, R. 1962 Unsteady natural convection in the vicinity of a doubly infinite vertical plate. *J. Heat Transfer* **84** (4), 334–338.

Shen, S. F. 1961 Some considerations on the laminar stability of time-dependent basic flows. *J. Aerospace Sciences* **28** (5), 397–404.

Squire, H. B. 1933 On the stability for three-dimensional disturbances of viscous fluid flow between parallel walls. *Proc. Royal Soc. Lond. Series A, Containing Papers of a Mathematical and Physical Character* **142** (847), 621–628.

Szewczyk, A. A. 1962 Stability and transition of the free-convection layer along a vertical flat plate. *Int. J. Heat Mass Transf.* **5** (10), 903–914.

Williamson, N., Armfield, S. W. & Kirkpatrick, M. P. 2012 Transition to oscillatory flow in a differentially heated cavity with a conducting partition. *J. Fluid Mech.* **693**, 93–114.

Williamson, N., Armfield, S. W., Lin, W. & Kirkpatrick, M. P. 2016 Stability and nusselt number scaling for inclined differentially heated cavity flow. *Int. J. Heat Mass Transf.* **97**, 787–793.

Wu, X. & Cowley, S. J. 1995 On the nonlinear evolution of instability modes in unsteady shear layers: the stokes layer as a paradigm. *Quart. J. Mech. Appl. Math.* **48** (2), 159–188.